Predictive energy management for a wind turbine with hybrid energy storage system

Enrique González-Rivera, Raúl Sarrias-Mena, Pablo García-Triviño and Luis M. Fernández-Ramírez

Published in:
International Journal of Energy Research, vol. 44, nº 3, pp. 2316-2331

DOI (link to publication from Publisher):
https://doi.org/10.1002/er.5082

Publication date:
2020

Document Version:
Accepted version

Citation for published version:
González-Rivera E, Sarrias-Mena R, García-Triviño P, Fernández-Ramírez LM. Predictive energy management for a wind turbine with hybrid energy storage system. Int J Energy Res. 2020; 44: 2316–2331. https://doi.org/10.1002/er.5082.

INTERNATIONAL JOURNAL OF
ENERGY RESEARCH

Predictive Energy Management for a Wind Turbine with Hybrid Energy Storage System

Journal:	*International Journal of Energy Research*
Manuscript ID	ER-19-12902.R1
Wiley - Manuscript type:	Research Article
Date Submitted by the Author:	02-Dec-2019
Complete List of Authors:	González-Rivera, Enrique; University of Cadiz Higher Polytechnic School of Algeciras, Electrical Engineering Sarrias-Mena, Raul; University of Cadiz Higher Polytechnic School of Algeciras, Engineering in Automation, Electronics and Computer Architecture & Networks garcia, pablo; University of Cadiz Higher Polytechnic School of Algeciras, Electrical Engineering Fernández-Ramírez, Luis M.; University of Cadiz Higher Polytechnic School of Algeciras, Electrical Engineering
Keywords:	Energy management system, energy storage, hybrid energy storage system, hydrogen storage, predictive control, supervisory control system, ultracapacitor

Predictive Energy Management for a Wind Turbine with Hybrid Energy Storage System

Enrique González-Rivera [a], Raúl Sarrias-Mena [b], Pablo García-Triviño [a], Luis M. Fernández-Ramírez [a]

[a] *Research Group in Electrical Technologies for Sustainable and Renewable Energy (PAIDI-TEP-023), Department of Electrical Engineering, University of Cadiz, 11202 EPS Algeciras, Algeciras (Cadiz), Spain; {enrique.gonzalezrivera; pablo.garcia; luis.fernandez}@uca.es*

[b] *Research Group in Electrical Technologies for Sustainable and Renewable Energy (PAIDI-TEP-023), Department of Engineering in Automation, Electronics and Computer Architecture & Networks, University of Cadiz, 11202 EPS Algeciras, Algeciras (Cadiz), Spain; raul.sarrias@uca.es*

Abstract

Hybrid energy storage systems (HESSs) help mitigating the fluctuations and variable availability of certain renewable sources, such as wind power, as they can provide support in different time scales. Therefore, regulating their state-of-charge (SOC) becomes crucial to ensure that the hybrid system complies with generation commitments agreed in time-ahead markets despite subsequent unexpected wind speed variations. So far, research has been mainly targeted at avoiding extreme SOC situations in the storage devices, whereas the regulation of this parameter to specific values has often been disregarded. A novel approach is proposed in this work, where model predictive control (MPC) is used to regulate the SOC of a HESS under variable wind and grid demand scenarios. The MPC-based supervisory controller developed for the hybrid system has been implemented and simulated under different situations. This controller monitors the future variation of the SOC with the aim of having the HESS available to develop its assigned functions successfully. The results show that a proper regulation of the SOC in the HESS increases the capacity to manage the active power supplied to the grid by the

hybrid system based on wind power, as well as the level of compliance with generation commitments established time ahead.

Keywords

Energy management system; predictive control; supervisory control system; energy storage; hybrid energy storage system; ultracapacitor; hydrogen storage; .

1. Introduction

Due to the growing participation of wind power and other renewable sources in power systems, technical and economic concerns arise associated to their inherent variability and unpredictability [1–4]. In this sense, energy storage systems (ESSs) are frequently considered a valuable complement to reduce the fluctuations of wind power generators [5–7]. Many large-scale ESSs can be used for such purposes. They are based on different physical principles, designed to perform various tasks, present dissimilar maturity, etc. In this work, a hybrid energy storage system (HESS) comprising two different storage technologies is used. One of the ESSs considered is the ultracapacitor (UC), which typically shows high charge and discharge speed, high efficiency and power density, very high cycle-life and low maintenance [8–10]. The second storage technology is a hydrogen system consisting of an electrolyzer (EZ) to produce hydrogen from electricity, a tank to store the hydrogen produced, and a fuel cell (FC) to generate electricity from hydrogen. The hydrogen system was chosen for its capacity to exchange large amounts of power for long periods [11,12]. In this sense, it allows time-shifting generation and demand, thus enhancing the integration of wind power generation in electric power systems. The objective of using a HESS is to exploit the differentiated characteristics of the two ESSs considered, since, for certain tasks, each of them will show a better performance than the other.

In hybrid power systems combining renewable sources and ESS, it becomes necessary to

design adequate control strategies for a sensible energy management [13,14]. Many different control techniques can achieve that goal. A review of optimal control strategies for supervisory control systems (SCS) and energy management systems (EMS) in microgrids was presented in [15]. As stated by the authors, among other alternatives, model predictive control (MPC) techniques can be used in microgrids to optimize the energy management between distributed energy sources and ESSs. An economic evaluation based on game theory for wind power generation − HESS was conducted in [16]. The main objective was to improve the power quality by smoothing the output power of the wind farm using a combination of batteries and UCs. The earnings of the wind power injection to the grid and the cost of the HESS were observed in the study. However, the regulation of the SOC of the storage devices was not considered, which is necessary to allow an increased availability of the HESS. Different methods to estimate the SOC of an ESS were proposed in [17,18]. Nevertheless, the performance of the ESS was not evaluated integrated under a more complex hybrid energy system. The use of UC as a means to improve the reliability and stability in electric power systems was addressed in [19], where a novel control technique was applied to reduce frequency variations and demand/generation power imbalance. The study did not consider the fluctuations introduced by renewable sources in the energy management. Another thorough review of SCS and EMS in microgrids was presented in [20]. The authors described hierarchical control structures and discussed the main characteristics of centralized and decentralized management to focus on optimal dispatching techniques and EMS in centralized configurations. A review of EMS in grids with renewable energies and ESS was also carried out in [21]. Different approaches were considered, with a specific mention to MPC and a revision of several papers on the topic.

Certain issues regarding accurate energy bifurcation in microgrids with several ESS were addressed in [22,23]. The concept of superimposing a DC virtual frequency was introduced in these references to overcome the difficulties derived from an energy management based on the

control of DC voltage. A virtual frequency-based droop technique was presented in [22] to reduce the power bifurcation error significantly, and minimize the undesired power circulation between the AC and DC sub-grids. In [23], a master-slave configuration of the individual controllers was proposed showing a satisfactory performance. The master converters were in charge of introducing the DC virtual frequency in the microgrid to improve the accuracy of the energy bifurcation. This superimposed virtual frequency was computed observing the SOC of the ESSs and the power demand. On the other hand, the slave converters used different ESS technologies to balance the power mismatch between demand and generation.

The development of predictive strategies to control hybrid energy systems was addressed in several studies [24–33]. In [24], the authors implemented an optimal control technique for an islanded microgrid based on non-linear MPC. The microgrid consisted of different renewable sources, battery energy storage, as well as residential and industrial loads. Optimal load shedding was performed by the predictive controller to avoid power imbalances, thus leaving some demand unaddressed in certain conditions. In [25], an economic MPC was used for the energy management of a microgrid system connected to the electric power grid. The authors used MPC to minimize the costs of energy generation and distribution while satisfying an established demand profile. In their configuration, the ESSs compensated the imbalances between generation and demand. The SOC of the ESS was introduced as a constraint in the optimization algorithm. Nevertheless, this parameter was not actively regulated, and the contribution of a diesel generator was necessary in some cases. Furthermore, uncertainties between the forecast and the actual power generation of the renewable sources were neglected. An energy system with various sources was studied in [26]. Electric storage was considered in the form of batteries in electric vehicles. The SOC of these batteries was introduced as a constraint in a MPC. Nevertheless, the coordinated operation of different ESSs in the same hybrid scheme was not evaluated. An approach to minimize energy consumption from the grid

through MPC was presented in [27]. In this case, a battery ESS supplied the necessary power to the hybrid system during periods of high demand, thus decreasing the energy purchase from the grid. A wind turbine (WT) and a local consumer were also present in the hybrid system. Nevertheless, the possibility to introduce an additional ESS capable of long energy exchanges was not observed, as this function was covered by the grid. A hybrid system with several ESSs working coordinated was evaluated in [28]. The authors proposed a MPC-based EMS for a hybrid system powering a tramway. The MPC was responsible for regulating the SOC of the battery and UC in the hybrid system close to their references, while being able to supply the known load profile of the tramway. This task was accomplished by setting the current references for the DC/DC converters that interconnect the ESSs. Nonetheless, the uncertainty introduced by renewable power generation was not an inconvenience in this configuration, since the ESSs were the only power sources fuelling the tramway. Furthermore, when an excess of energy surplus occurred in the hybrid system (e.g.: battery and UC fully charged), the absence of an EZ made it necessary to dissipate energy in a braking resistor at some periods. In [29], the authors employed distributed MPC to regulate the cooperation among several microgrids. With their approach, the authors conditioned the energy exchange between microgrids to an improvement of both the local (microgrid level) and the global (network of microgrids) status. Their main interest was the economic dispatch of several microgrids taking into consideration multiple aspects, whereas they did not particularly focus on the regulation of the SOC. A SOC-oriented control of a battery was presented in [30], where the charge/discharge rate of the ESS was modified linearly according to its SOC, and stopped at the maximum/minimum limits. In this sense, the authors focused on limiting the SOC of an ESS, rather than on its regulation. Furthermore, a single ESS was considered in [30], showing a limited ability to manage energy among different devices. This contrasts with the approach presented herein, where the SOC is actively regulated to a reference value by a smart EMS in

a HESS integrated by two different storage technologies. In [31], the authors compared three different types of stochastic MPC controllers to satisfy the power demanded by local consumers in a microgrid. The microgrid under study was a lab-scale system consisting of an emulated solar field, a battery bank, a hydrogen system and emulated local consumers. The MPC designed by the authors obtained successful results, keeping the SOC of the batteries and the level of the hydrogen tank near their references. However, the uncertain and highly fluctuating character of wind power generation was not included in this study. In [32], a hybrid configuration with batteries and UCs was evaluated. The authors proposed three individual explicit-MPC controllers for the total output current, battery and UC control loops. Experimental results proved that the proposed control strategy maintained the operation of the hybrid power source within the defined ranges. Nevertheless, the SOC of the ESSs was considered as a constraint to the optimization problem, instead of actively regulated to a reference value. The SOC of a UC within a hybrid system was controlled by an MPC algorithm in [33]. In this scheme, the UC was used, together with a FC stack, to power a construction vehicle. The authors considered the variation on the power demanded by the vehicle as the forecasting parameter in the MPC. However, renewable energy sources were not a part of this hybrid configuration, and their fluctuations were not present on the power generation side. The uncertainty of renewable sources were indeed observed in the robust MPC presented in [34]. Nevertheless, a single ESS was considered on the microgrid evaluated. Furthermore, controlling the SOC of the ESS was not within the duties of the EMS, as in other previously cited references.

In HESSs, the differentiated performance of each ESS is a highly valuable advantage, but also a challenge in terms of the energy management among them [35–37]. If the SOC of all the ESSs is not evaluated in mutual coordination, a situation may occur where one of the ESSs reaches its minimum/maximum SOC limitation, thus losing its availability as an energy backup,

while, at the same time, other ESSs in the hybrid system may be facing an opposite SOC. To avoid this undesired performance, it is sensible to manage energy within the hybrid system wisely and regulate the SOC of the ESSs involved. If this task is carried out successfully, the operation of the ESSs can be extended in time by avoiding limit SOC situations. An approach to complete this objective was presented in our previous work [38]. Nevertheless, the configuration presented herein differs from [38] in certain relevant aspects. First, the SCS implemented in [38] is based on an intelligent control technique, such as fuzzy logic, designed through an experience-based process, whereas the control strategy proposed in this work is based on MPC, a completely different concept that includes an optimization algorithm to find the best feasible solution. Furthermore, the SOC of the ESSs was regulated within a broad range of variation in [38], while specific values are used as SOC references herein. With this approach, the MPC allows a more precise regulation of the SOC. A SOC balancing strategy was presented in [39] based on a fuzzy tuned dynamic exponent technique. However, this article focused on the internal SOC equalization within the elements of a ESS, instead of among two ESSs with a dissimilar dynamic response. In this sense, the state of power regulation was considered in [40,41] together with a SOC equalization strategy, where ESSs with a quick and large power response were used to improve the transient response of a HESS. The state of power management was implemented in the ESS with fast response using a fuzzy logic-based PI controller.

In the configuration proposed in this paper, the WT is the primary power source, and it is connected to grid with the support of a HESS. In this HESS, the hydrogen system serves two purposes. Firstly, it allows time-shifting the wind power generation to adapt to a variable grid demand. Secondly, it helps regulating the SOC of the UC (SOC_{UC}), with lower capacity, to defined reference values. On the other hand, the fast and small deviations of the actual wind power generation from the predicted value are compensated by the UC. Subsequently, the

combined operation of both ESSs will allow the hybrid system to provide a controlled output power to the grid according to commitments established time ahead. Therefore, the main objectives of this work are: i) to design a SCS based on MPC that develops a smart energy management in the hybrid system; ii) to maintain the HESS at an adequate SOC to be able to match a fluctuating power generation from the WT with a variable demand from the transmission system operator (TSO); iii) to protect the UC from overcharge or complete depletion cycles that may jeopardize its proper operation, using the hydrogen ESS as a backup due to its higher energy capacity; iv) to provide a time-shifted and smooth power injection to the grid from a fluctuating renewable source.

Based on the previous review of the literature, the main contributions of this paper are:

1. Design of a smart energy management strategy in a hybrid system with wind power and a HESS. The SCS implemented allows regulating SOC_{UC} with the support of the hydrogen system. This reduces the risk of unavailability of the UC as a power regulation element because of maximum/minimum SOC situations.
2. The proposed SCS enhances the smart energy management in the hybrid system using the HESS with a dual purpose. Each of the two storage devices considered develops differentiated tasks in the regulation and control of the active power in the hybrid system. Additionally, those ESSs with larger capacity can support others with lower capacity to regulate their SOC and avoid full charge/discharge and subsequent loss of their availability. In this case, if SOC_{UC} is lower than desired, the hydrogen system can charge the UC. If SOC_{UC} is higher than desired, the excess energy can be converted into hydrogen instead of being wasted.
3. The proposed SCS considers SOC_{UC} as a control parameter rather than just as a constraint. This puts the focus on the proper regulation of this parameter and enhances the importance of having all ESSs available to control the total power injection of the hybrid system

satisfactorily.

4. The proposed SCS uses MPC to regulate SOC_{UC} to a specified value. Therefore, the amount of back-up energy that remains stored in this ESS in future intervals is actively controlled, instead of depending solely on the operating conditions. Anticipating the energy stored in the HESS allows operating the hybrid system in time-ahead markets similarly to traditional power plants. This opens the door to future designs where the desired SOC references could be calculated based on technical or economic optimization criteria, which is beyond the scope of this study.

The remainder of the paper is organized as follows: The configuration of the hybrid system, detailing the main elements, the structure, and the inputs and outputs considered, is described in Section 2. Sections 3 shows the modelling of the WT and ESSs. The characteristics of the SCS designed are presented in Section 4. Section 5 discusses the simulation results. Finally, the main findings are summarized in Section 6.

2. Configuration of the Hybrid System

The hybrid system proposed in this work consists of four elements. A WT acts as the principal power source. It operates in the maximum power point to maximize the energy captured from the wind. Additionally, a HESS is coupled to the WT as a secondary power source. This HESS increases the ability to manage and regulate the WT power generation, thus reducing the drawbacks of the fluctuating and intermittent power production of this green source. The WT drives a doubly-fed induction generator (DFIG). The storage devices are connected using bidirectional DC/DC power converters at the DC link of the DFIG. Hence, the power supplied by the HESS in DC is converted to AC using the grid-side converter (GSC) of the DFIG, avoiding the need for additional AC/DC conversion stages to inject the power provided by the ESSs to grid. The WT and the HESS must operate in coordination to achieve efficient energy exchanges within the hybrid system and with the grid. In this sense, a SCS has

been developed to provide the power references to the control systems of each power converter. The SCS proposed herein is based on a MPC technique, and it is detailed in Section 4.

Regarding the ESSs, two different technologies are considered. This configuration with a HESS presents relevant advantages, since the main features of each ESS can be considered to develop different functions in the hybrid system. In this sense, UCs have been chosen because of their satisfactory performance under fast and repeating charge/discharge cycles, and the hydrogen system, consisting of the FC and the EZ, because of the large amount of energy it can store for long periods. These characteristics are observed in the SCS implemented for a smart energy management.

The configuration of the hybrid system is sketched in Figure 1, which shows the main components and the control systems. As seen, the total active and reactive power outputs of the hybrid system are given by P_t and Q_t respectively.

3. Modelling of the Hybrid System

The detailed modelling of the elements comprising the hybrid system is presented in APPENDIX A. Nevertheless, the most relevant aspects are briefly described in this section.

The main power source of the hybrid system consists of a variable-speed WT driving a DFIG based on a 1.5 MW product by General Electric [42]. A fifth-order model is considered for this element, using the actuator disk theory for the wind turbine, and the two resonant masses model for the power train [43]. A PI-based control loop is implemented to limit the rotating speed by controlling the pitch angle of the blades. Furthermore, the rotor-side and grid-side converters (RSC and GSC respectively) of the DFIG are used to control the active power generation, the stator and GSC reactive power, and the voltage at the DC link [44], indicated as P_g, Q_s, Q_{GSC} and V_{DC}, in Figure 1. The 1.5 MW rated power of the DFIG is chosen as the base power for *per unit* conversions in the system.

Figure 1: Scheme of the hybrid configuration proposed.

Regarding the ESSs, they are modelled using well-known dynamic models valid for transient stability studies. The EZ is modelled through a controllable DC voltage source and an electrical resistance in series connection [45], using the parameters of the proton exchange membrane stack in [46] to implement a 350 kW EZ. The 450 kW FC model consists of a variable DC voltage source with a series-connected resistor that represents the internal losses of the device [47], and the hydrogen tank is modelled as the balance of mass flowing in and out the container. According to the configuration implemented, the hydrogen stored in the tank is provided by the EZ, whereas the hydrogen extracted from the tank is consumed in the FC. Finally, the UC model is built with an ideal capacitor and a resistor connected in series to account for the internal losses [48]. The parameters of product BMOD0063 P125 from Maxwell Technologies [49] have been used to configure an UC with a capacity of 2.5 kWh and a full-charge voltage of 625 V.

The connection of each storage device to the DC link of the DFIG is provided by bidirectional DC/DC buck-boost converters. These converters present two power electronic switches based on IGBT-diode switches working at 2.7 kHz. They also have a 0.4 mH inductor and a 0.3 mF capacitor at the ESS side, and a 1.1 mF capacitor at the DC-bus side, to reduce current and voltage ripples [50,51]. The control system for each ESS consists of a single PI control loop that tracks the active power reference defined by the SCS.

4. Supervisory Control System

In hybrid systems including different power sources and energy storage, a supervisory controller is typically needed to generate the active power references in order to manage energy efficiently. Therefore, a SCS that coordinates the operation of the DFIG, the EZ, the FC and the UC becomes necessary in the proposed hybrid configuration.

The first premise of the SCS developed herein is that the hybrid system has to satisfy the grid power demand. This demand may correspond to a previous agreement on day-ahead markets for the active power that the hybrid system will inject into the grid, in order to carry out an economic exploitation of the power plant. The hybrid system counts on two main tools to comply with this commitment. First, the power generation forecasts for the WT, which can help deciding the active power provided to the grid by the hybrid system for each period in day-ahead markets. Second, the HESS, which plays a crucial role as a secondary power source to support and regulate the total power injected to the grid. These two elements must be considered in the SCS to develop an efficient energy management within the components of the hybrid system.

The SCS conceived for this hybrid configuration is designed in two stages. In a first stage, three magnitudes are used to calculate the primary power references for the HESS: 1) the active power requested by the grid (P_{demand}); 2) the actual DFIG active power generation (P_g), calculated by adding the power exchange through the stator and rotor windings; and 3) a day-ahead estimation of the DFIG active power generation (P_{DFIG}^*). As previously described, P_{demand} can be set by the TSO according to a pre-established commitment agreed in day-ahead markets. Moreover, P_g is given by the DFIG model as a function of a fluctuating wind speed. Finally, P_{DFIG}^*can be obtained from wind speed forecasts and the DFIG active power curve [52]. The wind speed forecasting technique is not discussed nor developed in this paper because it is outside the scope of this work. Therefore, $P_{DFIG}^*$is used as a given input value.

If P_{demand} is the result of market agreements, it may remain constant for long periods (e.g. from several minutes up to an hour). Analogously, the wind speed predictions, and therefore P_{DFIG}^*, can also be considered as constant values in this time range. Subsequently, the result is that both parameters can show a stable pattern without fluctuations for several minutes. Additionally, these values should not necessarily match at all times, as the operator of the wind

farm might want to develop an economic exploitation of the generation by time-shifting generation and demand, using the ESSs to store energy during periods with a low cost of energy, and releasing the stored energy during peak periods with a higher income. To achieve that goal, ESSs with enough capacity to provide or absorb energy for long periods are necessary. Furthermore, since frequent fluctuations are not expected for these signals, a fast dynamic response of the ESSs is not required. In this sense, the hydrogen system is an adequate candidate for such task. Hence, the difference between P_{demand} and P_{DFIG}^{*} will be covered by the EZ and the FC in the first stage of the SCS. It has been reported in the literature that frequent start-up of hydrogen FCs can reduce their expected cycle-life [53]. Therefore, the minimum power references for both the FC and the EZ are set to small, non-zero, positive or negative values respectively, in order not to cease the operation of the devices completely.

Moreover, since the wind speed forecast is not 100% accurate, ESSs should be used to compensate the difference between P_g and P_{DFIG}^{*}. To take advantage of the fast response and satisfactory performance under frequent fluctuations of the UC, this is the ESS chosen for this task. Additionally, the UC is also responsible for covering the fast changes on the references of FC and EZ that they are not able to provide due to their slow dynamic response.

A new concern arises regarding the lower capacity of the UC compared to the hydrogen system. The problem now is to maintain SOC_{UC} at a certain level that can manage the active power imbalance between P_g and P_{DFIG}^{*}. If SOC_{UC} is excessively high/low, the UC cannot absorb/deliver the necessary energy, thus losing its ability to regulate the power imbalance. To address this problem, an active power term is computed through a MPC algorithm to monitor and support SOC_{UC} in the second stage of the proposed SCS. This additional active power term, namely $P_{support}$, can be positive or negative, and it is provided by the hydrogen system by absorbing or generating an additional active power injection to maintain SOC_{UC} close to a reference value. This contribution of the FC and the EZ is proposed as a means to avoid extreme

SOC_{UC}, which may hamper the UC contribution as the fast response power backup in the hybrid system.

Subsequently, the power references for the ESSs are calculated in the SCS according to (1) and (2):

$$P_{UC\,ref} = P_{primary\,UC} + P_{support} = P_{DFIG}^{*} - P_g + P_{support} \quad (1)$$

$$P_{H2\,ref} = P_{primary\,H2} - P_{support} = P_{demand} - P_{DFIG}^{*} - P_{support} \quad (2)$$

where $P_{primary\ UC}$ and $P_{primary\ H2}$ are the primary power references for the UC and the hydrogen system, calculated without the contribution of the MPC, whereas $P_{UC\,ref}$ and $P_{H2\,ref}$ are the final power references for the controllers of the ESSs. In the hydrogen system, the FC will provide the positive values of P_{H2}, whereas the negative values will be consumed in the EZ to produce hydrogen.

A scheme of the complete implementation of the SCS is depicted in Figure 1, where the calculation of the primary power references and the contribution of the MPC to compute $P_{support}$ can be observed. Furthermore, Figure 2 shows the complete flowchart that runs every control interval of 300 s to generate the $P_{support}$ needed to track the reference for SOC_{UC}. In this sense, when SOC_{UC} is below its reference, the UC needs to be charged, which requires a negative value of $P_{support}$. This implies a higher power injection of the FC or a lower power absorption in the EZ ($P_{H2\,ref} > P_{primary\,H2}$), depending on the operation state of the hydrogen system. In both cases, $P_{UC\ ref} < P_{primary\ UC}$ to enhance the UC charge. On the other hand, when $SOC_{UC} > SOC_{UC\,ref}$, the FC will deliver less power, or the EZ will absorb more ($P_{H2\,ref} < P_{primary\,H2}$), to accelerate the discharge of the UC, which will compensate this deficit or excess respectively. This is regulated by generating a positive $P_{support}$.

The MPC is an optimization control technique based on the prediction of the state of the system within a specified future horizon. The optimization is developed by minimizing a cost function over the prediction horizon. The optimization algorithm defines a trajectory of the

control output that achieves an adequate reference tracking for the estimated output. The Simulink Control Design™ [54] toolbox was used to generate a linear-time invariant (LTI) model of the system. The resulting LTI model, together with the system output and the control signal registered, are used in the MPC algorithm to infer the evolution of the system. The MPC algorithm solves a quadratic program (QP) optimization problem at each control interval. The solution defines the manipulated variable (MV) inputted to the system during a control interval.

Figure 2: Flowchart of the SCS.

The cost function, namely $J(z_k)$, is given in (3). It is computed as the sum of three terms that evaluate specific aspects of the MPC performance:

$$Min\ J(z_k) = J_y(z_k) + J_{\Delta u}(z_k) + J_c(z_k) \tag{3}$$

In this sense, $J_y(z_k)$ is the term for tracking the output reference, $J_{\Delta u}(z_k)$ is the term that limits the deviation of the MV, and $J_c(z_k)$ penalizes when the constraints must be relaxed to achieve a feasible solution for the optimization problem. Additionally, z_k is the decision delivered by the QP, given by (4), where p is the prediction horizon, and k is the current control interval:

$$z_k = \left[P_{support}(k|k) \quad P_{support}(k+1|k) \quad \cdots \quad P_{support}(k+p-1|k)\right] \tag{4}$$

Eqs. (5) – (7) show the calculation of the terms in (3), including the weights that are tuned in the controller for each application:

$$J_y(z_k) = \sum_{i=0}^{p} \left\{ w_{SOC_{UC}} \left[SOC_{UC\,ref}(k+i|k) - SOC_{UC}(k+i|k) \right] \right\}^2 \tag{5}$$

$$J_{\Delta u}(z_k) = \sum_{i=1}^{p-1} \left\{ w_{P_{support}} \left[P_{support}(k+i|k) - P_{support}(k+i-1|k) \right] \right\}^2 \tag{6}$$

$$J_c(z_k) = \rho \cdot \varepsilon_k^2 \tag{7}$$

where $SOC_{UC}(k+i|k)$ is the SOC_{UC} predicted at the *ith* prediction horizon step, $SOC_{UC\,ref}(k+i|k)$ is the reference value at the *ith* prediction horizon step, $w_{SOC\,UC}$ is the weight that penalizes the deviation from the output reference, $w_{Psupport}$ is the weight that penalizes the increases in the MV, ε_k is the slack variable at the control interval k, and ρ represents the penalty weight when the constraints are relaxed.

Certain constraints must be applied to the MPC that affect the inputs and outputs of the system. As a constraint to the measured output, SOC_{UC} is limited in the MPC algorithm between 10% and 90% to prevent the complete charge or discharge of the device. As a constraint to the MV, $P_{support}$ must satisfy the conditions given by (8) and (9) because of the limitations of the hydrogen system.

$$-350\ kW \le P_{H2} \le 450\ kW \tag{8}$$

$$\left(P_{demand} - P_{DFIG}^{*}\right) - 450\ kW \le P_{support} \le 350\ kW + \left(P_{demand} - P_{DFIG}^{*}\right) \tag{9}$$

The parameters and constraints of the MPC implemented are summarized in Table 1.

Table 1. Summary of the MPC parameters

A control interval T_s of 300 s is chosen because of the slow dynamic response of the hydrogen system, in order to reduce the number of changes on its power reference. A period of 300 s is enough for the EZ and FC to reach a new steady state after a step change on their references. The resulting MPC was evaluated through simulation changing the value of different parameters, obtaining a satisfactory performance.

5. Results and Discussion

The hybrid system presented herein is tested through simulation under various operating

conditions. The hybrid system without the MPC controller in the SCS is used as a benchmark to show the improvements achieved when the MPC is integrated in the SCS. Furthermore, two cases study are considered to evaluate the performance of the SCS with the MPC under two different control objectives. The first simulation shows the proper regulation of SOC_{UC} to a constant reference under changing conditions of the input parameters, whereas the second illustrates the response to a step change in the reference for SOC_{UC}. The results are discussed below.

5.1. Case Study 1: Constant SOC_{UC} Reference

This simulation evaluates the satisfactory regulation of SOC_{UC} when the inputs of the SCS change among different values. A wind speed fluctuating between 8.5 m/s and 11.5 m/s is considered. From (1) and (2), it can be seen that P_{DFIG}^{*} and P_{demand} are used in the SCS to compute $P_{UC\,ref}$ and $P_{H2\,ref}$. In this first simulation, these parameters vary as shown in Figure 3a. Therefore, these variations imply changes on the power references for the ESSs.

Even though the ESSs are connected at the DC link of the DFIG, the operation of the WT should not be affected by a changing active power injection of the storage devices, nor by the action of the MPC to generate the power support between the ESSs. In this simulation, it was observed that both configurations (with and without MPC) showed a similar response regarding the active power generation of the DFIG. Additionally, a constant voltage at the DC link of the DFIG is crucial to preserve the stability of the hybrid system. The results showed that this magnitude is adequately controlled at its command value, and the inclusion of the MPC in the SCS does not affect its performance.

As previously detailed, the hydrogen system is responsible for delivering or absorbing the difference between P_{DFIG}^{*} and P_{demand} in Figure 3a. This calculation is strictly valid for the system without MPC, whereas in the configuration with MPC, the term $P_{support}$ is defined to regulate SOC_{UC}. Figure 3b shows the active power exchanged by the hydrogen system for the

two SCSs compared. In both configurations P_{H2} starts increasing from the beginning of the simulation due to the initial mismatch between P_{DFIG}^* and P_{demand}, which implies a $P_{primary\ H2}$ equal to 0.2 pu. For the SCS without MPC, it can be clearly seen that the FC provides 0.2 pu during the first 15 min of the simulation, which corresponds to the difference between P_{demand} and P_{DFIG}^* in this interval. Between 15 min and 30 min, this difference becomes zero, and neither the FC nor the EZ exchange active power if the MPC is not present. From 30 min until the end of the simulation, P_{DFIG}^* becomes higher than P_{demand}, and the EZ is responsible for using this excess of generation to produce hydrogen.

On the other hand, with the MPC in the SCS, the primary references of the FC and the EZ are modified to provide additional support to the UC. The hydrogen system is required to deliver or store additional power than just the necessary to cover the prediction vs. demand imbalance. Hence, every 300 s the MPC calculates $P_{support}$ and modifies the primary power references for the FC and the EZ. Subsequently, certain differences can be observed between the SCS with and without MPC in Figure 3b. These differences correspond to the $P_{support}$ calculated to regulate SOC_{UC}. The effects of $P_{support}$ in the EZ and the FC were described in Section 4. In this regard, the situations that occur from 5 min to 15 min, and from 20 min to 30 min are certainly clarifying. In the period from 5 min to 15 min, SOC_{UC} has increased above its reference. Therefore, the configuration with MPC tries to reduce SOC_{UC} to track its reference. This is accomplished using the UC instead of the hydrogen system to supply the mismatch between P_{demand} and P_{DFIG}^*. As a consequence, the hydrogen system is freed from this task, reducing its output power, and increasing the output power of the UC. Hence, SOC_{UC} decreases and approaches its reference in the configuration with MPC. On the other hand, after a transitory response, the hydrogen system does not exchange any active power with the grid between 20 min and 30 min, since P_{DFIG}^* and P_{demand} are set at the same value. However, a small power consumption in the EZ is registered in the SCS with MPC due to the UC discharge

needed to regulate SOC_{UC} closer to its reference. The power that has to be extracted from the UC to reduce its SOC cannot be delivered to the grid not to deviate P_t from P_{demand}. Hence, the additional discharge of the UC is consumed in the EZ to produce hydrogen. Therefore, a smart use of the excess of energy stored in the UC was accomplished with the MPC strategy.

The contribution of $P_{support}$ is also appreciated in P_{UC}, shown in Figure 3c. In the configuration without MPC, the UC output power is only responsible for compensating the power imbalance between P_g and P_{DFIG}^*. As P_g varies with wind, P_{UC} shows fast and frequent fluctuations. Such behaviour could not be achieved by the hydrogen system due to its slower dynamics and poor performance in highly fluctuating operation. As seen in Figure 3c, positive values of $P_{support}$ imply higher discharge/lower charge for the UC, whereas the consequence of a negative $P_{support}$ is the opposite. This effect can be also observed in Figure 4a. During periods with a negative $P_{support}$, SOC_{UC} in the configuration with MPC increases faster than in the configuration without MPC. Analogously, when a decrease on SOC_{UC} is necessary, the MPC generates a positive $P_{support}$ to favour the discharge of the UC.

The results illustrated in Figure 4a clearly show that the configuration with MPC in the SCS is able to regulate SOC_{UC} close to a specified value. Even though the operating conditions (i.e. P_{DFIG}^*, the wind speed, or P_{demand}) vary, the MPC generates the necessary $P_{support}$ that manages the active power exchange between the ESSs to monitor SOC_{UC}, avoiding situations that could potentially damage the UC. Under the same operating conditions, the configuration without MPC reaches a maximum SOC_{UC} close to 120%, as there is no regulation mechanism for this parameter. A SOC_{UC} around 120% means that the voltage applied to the UC terminals is approximately 20% higher than the rated value. This undesired situation should be avoided to minimize the risk of damaging the device. As shown, the SCS with MPC achieves a successful regulation under different operating conditions.

As it could be expected, the contribution of the MPC in the SCS also shows certain effects

on the level of hydrogen in the tank. It can be observed in Figure 4b that the level of the hydrogen tank in the configuration with MPC is higher than in the configuration without MPC for most of the simulation. This is a consequence of the previously described behaviour of the UC. Since the MPC avoids an excessively high charge of the UC, the excess of energy in the UC is consumed in the EZ, thus increasing the hydrogen generation compared to the configuration without MPC. Therefore, the MPC proved a double benefit in this simulation. On the one hand, it helped regulating SOC_{UC} around an established reference, allowing a safer operation of this device. On the other hand, the MPC developed a smart energy management within the hybrid system, since the excess of energy rejected by the UC during the regulation of SOC_{UC} was moved to the EZ, thus accomplishing an intelligent use of the available energy.

Figure 3: Results of case study 1: a) DFIG power generation forecast and P_{demand}; b) Hydrogen system output power and $P_{support}$; c) UC output power and $P_{support}$.

Figure 4: Results of case study 1 (cont.): a) SOC of the UC; b) Level of the hydrogen tank; c) Total output power of the hybrid system.

The improved performance of the SCS with MPC is finally demonstrated in Figure 4c, where P_t (i.e. the active power injected to the grid by the hybrid system) is represented. As seen, the SCS without MPC is not able to match P_{demand} by the end of the simulation. This is a consequence of the low SOC_{UC} registered during this period, as shown in Figure 4a, which reduces the contribution of P_{UC} to zero (Figure 3c). Moreover, since the UC cannot filter the power fluctuations due to its low SOC, these fluctuations are transferred to the output power, as observed in the configuration without MPC. In contrast, the SCS with MPC developed an adequate regulation of SOC_{UC} and satisfied the grid demand during the whole simulation. This

result proves the main benefit achieved by the SCS with MPC, since a smarter management of the energy available in the hybrid system allows increasing the capacity to provide a controlled power output from a renewable resource.

5.2. Case Study 2: Change in SOC_{UC} Reference

To validate the adequate regulation of SOC_{UC}, a second scenario is simulated with a step change on the reference for this parameter. In this situation, the MPC must be able to regulate SOC_{UC} to two different values throughout the simulation. To clearly differentiate the effects of changes in the reference for SOC_{UC} from the effects of changes in other inputs (shown in the previous case study), $P_{DFIG}{}^{*}$ is kept constant at 0.55 pu, whereas a single step change is introduced for P_{demand} at 40 min from 0.47 pu (700 kW) to 0.6 pu (900 kW). Additionally, the reference for SOC_{UC} is set at 50% at the beginning of the simulation, and changes at 30 min to 75%. The same fluctuating wind speed as in the previous case study is used.

Under these conditions, the SCS with MPC is able to regulate SOC_{UC} to the reference values defined, as seen in Figure 5a. The configuration with MPC controls SOC_{UC} to 50% during the first half of the simulation. Since the MPC is generating a new value of $P_{support}$ every 300 s, it takes some time for the controlled variable to reach the reference value. Nevertheless, a clear tendency towards 50% can be observed, in contrast with the configuration without MPC, which is not able to regulate SOC_{UC}. Therefore, in the configuration without MPC, SOC_{UC} varies as a result of the UC charge and discharge according to the primary reference set in the first stage of the SCS. For the last 30 min of the simulation, the SCS with MPC drives SOC_{UC} to its new reference at 75%, whereas the configuration without MPC cannot regulate this parameter and it decreases at its minimum recommended value for some periods. Furthermore, the change in P_{demand} at 40 min does not affect the behaviour of the system with MPC. Therefore, these results show the adequate performance of the MPC implemented in the SCS to control SOC_{UC} under different operating conditions.

The output power of the UC for each configuration is shown in Figure 5b. The effect of $P_{support}$ can be observed throughout the simulation. At the beginning, and from 30 min until 35 min approximately, P_{UC} is lower in the configuration with MPC than in the SCS without MPC. This additional energy consumption of the UC with MPC causes a significant increase on its SOC, as shown in Figure 5a. In other periods (e.g.: from 5 min to 15 min), P_{UC} is slightly higher for the SCS with MPC, and thus SOC_{UC} decreases faster than in the case without MPC. These differences between both configurations are caused by the contribution of $P_{support}$ in the SCS with MPC. Hence, when $P_{support}$ is negative, the UC is charged faster, whereas positive values of $P_{support}$ imply a higher discharge of the device. When the MPC is not present, the UC only compensates the difference between P_g and P_{DFIG}^*, and SOC_{UC} varies accordingly. As observed in Figure 5a, from 42 min until the end of the simulation, there are some intervals where the UC is fully discharged. Subsequently, P_{UC} is zero for those periods in Figure 5b, and this device is not able to compensate the deviations between P_g and P_{DFIG}^*. This causes a major drawback when observed from the perspective of the grid. As seen in Figure 5c, during those periods of depleted UC in the SCS without MPC, the UC cannot filter the fluctuations of the DFIG power generation, and these fluctuations are transferred to the power injected to the grid. On the other hand, when the MPC is implemented on the SCS, SOC_{UC} is controlled and it does not lose the capacity to filter the fluctuations of the power generated by the DFIG. Therefore, the power injected to the grid by the hybrid system with MPC is able to follow the changing P_{demand} due to the contribution of the hydrogen system, as well as to smooth out the fluctuations of P_g by regulating SOC_{UC}. As shown, this is not feasible in the SCS without MPC.

Figure 5: Results of case study 2: a) SOC of the UC; b) UC output power and $P_{support}$; c) Total output power of the hybrid system and grid demand.

The active power exchanged by the hydrogen system is shown in Figure 6a. According to the design of the SCS, the hydrogen system is primarily in charge of covering the power imbalance between P_{DFIG}^{*} and P_{demand}. In this case, that power imbalance corresponds to a step change from -0.08 pu to 0.05 pu approx. at 40 min, and this is the power reference achieved in the SCS without MPC. Nonetheless, the SCS with MPC generates $P_{support}$ to regulate SOC_{UC}. This additional power term is exchanged between the UC and the hydrogen system. Therefore, it affects the power delivered or absorbed by the FC and the EZ respectively. This can be observed in Figure 6a, where the FC contributes to charge the UC during the first 5 min of the simulation and from 30 min to 35 min. On the other hand, from 5 min to 15 min and from 37 min to 40 min approximately, the EZ consumes more power to achieve a higher reduction of SOC_{UC}. This relation between the output/input power of the hydrogen system and SOC_{UC} was also highlighted in Figure 5a, thus proving the contribution of the hydrogen system on the regulation of SOC_{UC}. Such operation also brings differences to the amount of hydrogen stored in the tank, which is illustrated in Figure 6b. As observed, the level of the hydrogen tank is lower for the configuration with MPC, mainly due to the first 5 min of the simulation, when the SCS with MPC is consuming hydrogen in the FC to increase SOC_{UC}, whereas the SCS without MPC is producing hydrogen in the EZ during this period. This initial situation, together with the interval from 30 min to 35 min where the same situation occurs, penalizes the level of hydrogen in the tank for the rest of the simulation in the SCS with MPC, which is not compensated by the larger generation of the EZ in certain periods. Nevertheless, this lower level of the hydrogen tank is a minor disadvantage compared to the relevant benefit obtained with the MPC regarding the improved control of SOC_{UC} and the controllable active power injection to grid.

This second case study showed an improved performance of the SCS with MPC regarding the regulation of SOC_{UC} that, in the end, is translated into a higher quality of the power injected

to the grid by the hybrid system. Furthermore, it proved that the MPC can regulate SOC_{UC} to different values, which can be useful in applications where this reference is defined based on specific criteria.

Figure 6: Results of case study 2 (cont.): a) Hydrogen system output power and $P_{support}$; b) Level of the hydrogen tank.

6. Conclusions

This paper presented the design, modelling and simulation of a MPC-based SCS for a hybrid system coupling a WT and two large-scale ESSs. A HESS was implemented for energy management and power quality purposes. In this regard, the UC compensated fast and frequent fluctuations of the WT active power generation, whereas a hydrogen system was used for longer energy exchanges with the grid.

The MPC-based SCS was tested through simulation and compared with a SCS without the MPC strategy. The results showed a smarter energy management in the hybrid system for the configuration with MPC. The proposed configuration achieved an improved regulation of SOC_{UC} and longer HESS operation compared to the configuration without MPC. Subsequently, the energy regulation and output power smoothing capabilities of the HESS were enhanced by the MPC-based SCS. Additionally, overcharge and complete discharge of the UC were avoided using the hydrogen system as an energy backup when necessary, which protected the UC from potentially harmful situations. Finally, the variable power demanded by the TSO was successfully fulfilled by the hybrid WT with HESS system. As observed, a controlled and smooth power injection was provided due to the contribution of the proposed SCS based on MPC.

Acknowledgements

The authors acknowledge the Regional Government of Andalucía for their contribution under the Programme "Convocatoria para la Contratación de Joven Personal Investigador en el Marco del Sistema Nacional de Garantía Juvenil y del Programa Operativo de Empleo Juvenil"

Appendix A

A.1: Modelling of the Wind Turbine

The DFIG model is implemented using the voltage at the stator and rotor windings in the synchronous *dq* reference frame, as in (A1) and (A2):

$$\begin{aligned} u_{ds} &= R_s \cdot i_{ds} + \frac{d}{dt}\varphi_{ds} - \omega \cdot \varphi_{qs} \\ u_{qs} &= R_s \cdot i_{qs} + \frac{d}{dt}\varphi_{qs} + \omega \cdot \varphi_{ds} \end{aligned} \tag{A1}$$

$$\begin{aligned} u_{dr} &= R_r \cdot i_{dr} + \frac{d}{dt}\varphi_{dr} - (\omega - \omega_r) \cdot \varphi_{qr} \\ u_{qr} &= R_r \cdot i_{qr} + \frac{d}{dt}\varphi_{qr} + (\omega - \omega_r) \cdot \varphi_{dr} \end{aligned} \tag{A2}$$

where u stands for voltage, i for current, R for resistance, φ for magnetic flux, ω for angular speed, and subscript r stands for rotor variables and s for stator.

Additionally, the electromagnetic torque is given by (A3), where p indicates the pairs of poles:

$$T_e = 1.5 \cdot p \cdot (\varphi_{ds} \cdot i_{qs} - \varphi_{qs} \cdot i_{ds}) \tag{A3}$$

A.2: Modelling of the Electrolyzer

The hydrogen produced in the EZ, namely n_{H2}, is determined by the Faraday's law given by (A4):

$$n_{H2} = \frac{n_c \cdot I_{EZ}}{2 \cdot F} \cdot \eta_F \quad \text{(A4)}$$

where n_c is the number of cells connected in series, I_{EZ} is the input current of the EZ, F is the Faraday constant, and η_F is the Faraday efficiency, which can be obtained from the EZ current I_{EZ} as in (A5):

$$\eta_F = 96.5 \cdot exp\left(\frac{0.09}{I_{EZ}} - \frac{75.5}{I_{EZ}^2}\right) \quad \text{(A5)}$$

These two equations, plus the electrical performance as a linear variation of the output voltage with the input current, provide a valid model of this device.

A.3: Modelling of the Fuel Cell

The fuel cell terminal voltage (U_{FC}) is calculated as a function of several design parameters according to (A6):

$$U_{FC} = E_{FC} - R_i \cdot I_{FC} \quad \text{(A6)}$$

where I_{FC} is the instantaneous current of the FC, R_i is the internal resistance of the device, and E_{FC} is the value of the controlled DC voltage source calculated from (A7):

$$E_{FC} = E_{oc} - N \cdot A \cdot ln\left(\frac{I_{FC}}{i_0}\right) \quad \text{(A7)}$$

where E_{oc} is the open-circuit voltage, N is the number of cells connected in series, A is the slope in the linear region of the polarization curve (Tafel slope), and i_0 is an exchange current resulting from the continuous backward and forward flow of electrons from and to the electrolyte produced at no load conditions [55].

A.4: Modelling of the Hydrogen Tank

The level of hydrogen in the tank in percentage is given by (A8) and (A9):

$$L_{tank} = \left(M_{H2} + M_0\right) \cdot \frac{100}{C_{tank}} \quad \text{(A8)}$$

$$\frac{d}{dt} M_{H2} = m_{H2\,in} - m_{H2\,out} \quad \text{(A9)}$$

where L_{tank} is the level of hydrogen in the tank in percentage, M_0 is the initial mass in the tank in kg, C_{tank} is the total capacity of the container, M_{H2} is the mass of hydrogen in the tank, and the mass flows of hydrogen in and out of the tank are given in kg·s^{-1} by $m_{H2\,in}$ and $m_{H2\,out}$ respectively.

A.5: Modelling of the Ultracapacitor

The terminal voltage of the series UC branch, namely V_{UC}, is given by (A10):

$$V_{UC} = V_{UC0} - \frac{I_{UC}}{C_{UC}} \cdot t - R_{UC} \cdot I_{UC} \quad \text{(A10)}$$

where V_{UC0} is the initial UC voltage, R_{UC} represents the internal resistance of the UC and C_{UC} its capacity, and I_{UC} is the current in the branch.

In an UC, the SOC is directly proportional to the instantaneous terminal voltage V_{UC}, and inversely proportional to the rated voltage of the device $V_{UC\ rated}$. Thus, SOC_{UC} is given by (A11) in this work:

$$SOC_{UC}(\%) = \frac{V_{UC}}{V_{UC\ rated}} \cdot 100 \quad \text{(A11)}$$

Appendix B

The characteristics of the hybrid system presented in this paper are summarized in Table B.1.

Table B.1. Parameters of the hybrid system

References

[1] Akhmatov V, Knudsen H. Large penetration of wind and dispersed generation into

Danish power grid. Electr Power Syst Res 2007;77:1228–38. https://doi.org/10.1016/j.epsr.2006.08.009.

[2] Teleke S, Baran ME, Huang AQ, Bhattacharya S, Anderson L. Control strategies for battery energy storage for wind farm dispatching. IEEE Trans Energy Convers 2009;24:725–32. https://doi.org/10.1109/TEC.2009.2016000.

[3] Antonelli M, Desideri U, Franco A. Effects of large scale penetration of renewables: The Italian case in the years 2008–2015. Renew Sustain Energy Rev 2018;81:3090–100. https://doi.org/10.1016/j.rser.2017.08.081.

[4] Gerber A, Qadrdan M, Chaudry M, Ekanayake J, Jenkins N. A 2020 GB transmission network study using dispersed wind farm power output. Renew Energy 2012;37:124–32. https://doi.org/10.1016/j.renene.2011.06.004.

[5] Beaudin M, Zareipour H, Schellenberglabe A, Rosehart W. Energy storage for mitigating the variability of renewable electricity sources: An updated review. Energy Sustain Dev 2010;14:302–14. https://doi.org/10.1016/j.esd.2010.09.007.

[6] Huang Y, Keatley P, Chen HS, Zhang XJ, Rolfe A, Hewitt NJ. Techno-economic study of compressed air energy storage systems for the grid integration of wind power. Int J Energy Res 2018;42:559–69. https://doi.org/10.1002/er.3840.

[7] Yang WJ, Aydin O. Wind energy-hydrogen storage hybrid power generation. Int J Energy Res 2001;25:449–63. https://doi.org/10.1002/er.696.

[8] Hadjipaschalis I, Poullikkas A, Efthimiou V. Overview of current and future energy storage technologies for electric power applications. Renew Sustain Energy Rev 2009;13:1513–22. https://doi.org/10.1016/j.rser.2008.09.028.

[9] Aneke M, Wang M. Energy storage technologies and real life applications - A state of the art review. Appl Energy 2016;179:350–77. https://doi.org/10.1016/j.apenergy.2016.06.097.

[10] Xun Q, Liu Y. Evaluation of fluctuating voltage topology with fuel cells and supercapacitors for automotive applications. Int J Energy Res 2019:4807–19. https://doi.org/10.1002/er.4622.

[11] Díaz-González F, Sumper A, Gomis-Bellmunt O, Villafáfila-Robles R. A review of energy storage technologies for wind power applications. Renew Sustain Energy Rev 2012;16:2154–71. https://doi.org/10.1016/j.rser.2012.01.029.

[12] Luo X, Wang J, Dooner M, Clarke J. Overview of current development in electrical energy storage technologies and the application potential in power system operation. Appl Energy 2015;137:511–36. https://doi.org/10.1016/j.apenergy.2014.09.081.

[13] Chauhan A, Saini RP. A review on Integrated Renewable Energy System based power generation for stand-alone applications: Configurations, storage options, sizing methodologies and control. Renew Sustain Energy Rev 2014;38:99–120. https://doi.org/10.1016/j.rser.2014.05.079.

[14] Vivas FJ, De las Heras A, Segura F, Andújar JM. A review of energy management strategies for renewable hybrid energy systems with hydrogen backup. Renew Sustain Energy Rev 2018;82:126–55. https://doi.org/10.1016/j.rser.2017.09.014.

[15] Minchala-Avila LI, Garza-Castañón LE, Vargas-Martínez A, Zhang Y. A review of optimal control techniques applied to the energy management and control of microgrids. Procedia Comput Sci 2015;52:780–7. https://doi.org/10.1016/j.procs.2015.05.133.

[16] Han X, Zhao Z, Li J, Ji T. Economic evaluation for wind power generation–hybrid energy storage system based on game theory. Int J Energy Res 2017;41:49–62. https://doi.org/10.1002/er.3591.

[17] Zhang C, Zhu Y, Dong G, Wei J. Data-driven lithium-ion battery states estimation using neural networks and particle filtering. Int J Energy Res 2019:8230–41. https://doi.org/10.1002/er.4820.

[18] Ren H, Zhao Y, Chen S, Yang L. A comparative study of lumped equivalent circuit models of a lithium battery for state of charge prediction. Int J Energy Res 2019:7306–15. https://doi.org/10.1002/er.4759.

[19] Arya Y. Impact of ultra-capacitor on automatic generation control of electric energy systems using an optimal FFOID controller. Int J Energy Res 2019:8765–78. https://doi.org/10.1002/er.4767.

[20] Meng L, Sanseverino ER, Luna A, Dragicevic T, Vasquez JC, Guerrero JM. Microgrid supervisory controllers and energy management systems: A literature review. Renew Sustain Energy Rev 2016;60:1263–73. https://doi.org/10.1016/j.rser.2016.03.003.

[21] Zia MF, Elbouchikhi E, Benbouzid M. Microgrids energy management systems: A critical review on methods, solutions, and prospects. Appl Energy 2018;222:1033–55. https://doi.org/10.1016/j.apenergy.2018.04.103.

[22] Bhowmik P, Chandak S, Rout PK. Frequency superimposed energy bifurcation technology for a hybrid microgrid. Sustain Cities Soc 2019;45:607–18. https://doi.org/10.1016/j.scs.2018.12.027.

[23] Bhowmik P, Rout PK. Frequency superimposed robust coordinated control in a hybrid microgrid. Sustain Cities Soc 2019;51:101791.

https://doi.org/10.1016/j.scs.2019.101791.

[24] Minchala-Avila LI, Garza-Castanon L, Zhang Y, Ferrer HJA. Optimal energy management for stable operation of an islanded microgrid. IEEE Trans Ind Informatics 2016;12:1361–70. https://doi.org/10.1109/TII.2016.2569525.

[25] Nassourou M, Puig V, Blesa J, Ocampo-Martinez C. Economic model predictive control for energy dispatch of a smart micro-grid system. Proc. Int. Conf. Control. Decis. Inf. Technol., vol. 2017- Janua, Barcelona, Spain: 2017, p. 944–9. https://doi.org/10.1109/CoDIT.2017.8102719.

[26] Halvgaard R. Model Predictive Control for Smart Energy Systems. Technical University of Denmark, 2014. https://doi.org/10.1109/TSG.2016.2526077.

[27] Prodan I, Zio E. A model predictive control framework for reliable microgrid energy management. Int J Electr Power Energy Syst 2014;61:399–409. https://doi.org/10.1016/j.ijepes.2014.03.017.

[28] Torreglosa J, García P, Fernández L, Jurado F. Predictive control for the energy management of a fuel cell-battery-supercapacitor tramway. IEEE Trans Ind Informatics 2013;10:1–1. https://doi.org/10.1109/TII.2013.2245140.

[29] García-Torres F, Bordons C, Ridao MA. Optimal economic schedule for a network of microgrids with hybrid energy storage system using distributed model predictive control. IEEE Trans Ind Electron 2019;66:1919–29. https://doi.org/10.1109/TIE.2018.2826476.

[30] Hu J, Xu Y, Wai K, Guerrero JM. A model predictive control strategy of PV-Battery microgrid under variable power generations and load conditions. Appl Energy 2018;221:195–203. https://doi.org/10.1016/j.apenergy.2018.03.085.

[31] Velarde P, Valverde L, Maestre JM, Ocampo-Martinez C, Bordons C. On the comparison of stochastic model predictive control strategies applied to a hydrogen-based microgrid. J Power Sources 2017;343:161–73. https://doi.org/10.1016/j.jpowsour.2017.01.015.

[32] Hredzak B, Agelidis VG, Demetriades G. Application of explicit model predictive control to a hybrid battery-ultracapacitor power source. J Power Sources 2015;277:84–94. https://doi.org/10.1016/j.jpowsour.2014.11.148.

[33] Li T, Liu H, Ding D. Predictive energy management of fuel cell supercapacitor hybrid construction equipment. Energy 2018;149:718–29. https://doi.org/10.1016/j.energy.2018.02.101.

[34] Zhang Y, Fu L, Zhu W, Bao X, Liu C. Robust model predictive control for optimal energy management of island microgrids with uncertainties. Energy 2018;164:1229–41. https://doi.org/10.1016/j.energy.2018.08.200.

[35] Faisal M, Hannan MA, Ker PJ, Hussain A, Bin Mansor M, Blaabjerg F. Review of energy storage system technologies in microgrid applications: Issues and challenges. IEEE Access 2018;6:35143–64. https://doi.org/10.1109/ACCESS.2018.2841407.

[36] Jiang W, Zhang L, Zhao H, Huang H, Hu R. Research on power sharing strategy of hybrid energy storage system in photovoltaic power station based on multi-objective optimisation. IET Renew Power Gener 2016;10:575–83. https://doi.org/10.1049/iet-rpg.2015.0199.

[37] Sun C, Sun F, Moura SJ. Nonlinear predictive energy management of residential buildings with photovoltaics & batteries. J Power Sources 2016;325:723–31. https://doi.org/10.1016/j.jpowsour.2016.06.076.

[38] Sarrias-Mena R, Fernández-Ramírez LM, García-Vázquez CA, Jurado F. Design of a Supervisory Control System based on fuzzy logic for a hybrid system comprising wind power, battery and ultracapacitor energy storage system. Adv. Control Optim. Paradig. Wind Energy Syst., Singapore: Springer; 2019, p. 189–212. https://doi.org/10.1007/978-981-13-5995-8_8.

[39] Bhowmik P, Chandak S, Rout PK. State of charge and state of power management among the energy storage systems by the fuzzy tuned dynamic exponent and the dynamic PI controller. J Energy Storage 2018;19:348–63. https://doi.org/10.1016/j.est.2018.08.004.

[40] Bhowmik P, Chandak S, Rout PK. State of charge and state of power management of the hybrid energy storage system in an architecture of microgrid. J Renew Sustain Energy 2019;11. https://doi.org/10.1063/1.5053567.

[41] Bhowmik P, Chandak S, Rout PK. State of charge and state of power management in a hybrid energy storage system by the self-tuned dynamic exponent and the fuzzy-based dynamic PI controller. Int Trans Electr Energy Syst 2019;29:1–26. https://doi.org/10.1002/2050-7038.2848.

[42] General Electric. 1.5 - 77 Wind Turbine. GE Prod 2013. https://www.ge.com/in/wind-energy/1.5-MW-wind-turbine (accessed April 17, 2019).

[43] Heier S. Grid integration of wind energy conversion systems. West Sussex, UK: John Wiley & Sons, Ltd.; 2014. https://doi.org/10.1002/9781118703274.

[44] Sarrias-Mena R, Fernández-Ramírez LM, García-Vázquez CA, Jurado F. Fuzzy logic based power management strategy of a multi-MW doubly-fed induction generator wind turbine with battery and ultracapacitor. Energy 2014;70:561–76.

https://doi.org/10.1016/j.energy.2014.04.049.

[45] Sarrias-Mena R, Fernández-Ramírez LM, García-Vázquez CA, Jurado F. Electrolyzer models for hydrogen production from wind energy systems. Int J Hydrogen Energy 2015;40:2927–38. https://doi.org/10.1016/j.ijhydene.2014.12.125.

[46] Marangio F, Santarelli M, Cali M. Theoretical model and experimental analysis of a high pressure PEM water electrolyser for hydrogen production. Int J Hydrogen Energy 2009;34:1143–58. https://doi.org/10.1016/j.ijhydene.2008.11.083.

[47] Njoya SM, Tremblay O, Dessaint L-A. A generic fuel cell model for the simulation of fuel cell vehicles. Proc. IEEE Veh. Power Propuls. Conf., Dearborn, USA: 2009, p. 1722–9. https://doi.org/10.1109/VPPC.2009.5289692.

[48] Wei L, Joos G, Belanger J. Real-time simulation of a wind turbine generator coupled with a battery supercapacitor energy storage system. IEEE Trans Ind Electron 2010;57:1137–45. https://doi.org/10.1109/TIE.2009.2037103.

[49] Maxwell Technologies. Products catalog n.d. http://www.maxwell.com/images/documents/MANUAL_HTM125_20BMOD0063_1014343_8.pdf (accessed April 17, 2019).

[50] Tamalouzt S, Benyahia N, Rekioua T, Rekioua D, Abdessemed R. Performances analysis of WT-DFIG with PV and fuel cell hybrid power sources system associated with hydrogen storage hybrid energy system. Int J Hydrogen Energy 2016;41:21006–21. https://doi.org/10.1016/j.ijhydene.2016.06.163.

[51] Rahim AHMA, Nowicki EP. Supercapacitor energy storage system for fault ride-through of a DFIG wind generation system. Energy Convers Manag 2012;59:96–102. https://doi.org/10.1016/j.enconman.2012.03.003.

[52] Kavasseri RG, Seetharaman K. Day-ahead wind speed forecasting using f-ARIMA models. Renew Energy 2009;34:1388–93. https://doi.org/10.1016/j.renene.2008.09.006.

[53] Hajizadeh A, Soltani M, Norum LE. Intelligent power control of DC microgrid. Proc. IEEE Int. Conf. Ubiquitous Wirel. Broadband, Salamanca, Spain: 2017. https://doi.org/10.1109/ICUWB.2017.8251006.

[54] The MathWorks Inc. Simulink Control Design TM: User's guide. 2019.

[55] Rashid M. Power Electronics Handbook. 4th ed. 2017.

Table 2. Summary of the MPC parameters

Controller parameters		
Control interval (s)		300
Prediction horizon (intervals)		3
Control horizon (intervals)		2
Output Weights		
$w_{SOC_{UC}}$		3
Input Rate Weights		
$w_{P_{support}}$		0.01
Constraints		
Parameter	**Type**	**Range**
SOC_{UC} (%)	Level limitation	[10,90]
$P_{support}$ (kW)	Level limitation	Eq. 9

Table B.1. Parameters of the hybrid system

Wind Turbine		**Electrolyzer**		**Ultracapacitor**	
Rated power	1.5 MW	Rated power	350 kW	Rated capacity	2.5 kWh
Rated voltage	575 V	Rated voltage	590 V	Rated voltage	625 V
Rated freq.	60 Hz	n_c	400	R_{UC}	1.5 mΩ
Filter resist.	3 mΩ	Internal resist.	1.65 Ω	C_{UC}	756 F
Filter inductor	300 mH	**Fuel Cell**			
R_s	25 mΩ	Rated power	450 kW		
L_s	200 mH	E_{oc}	625 V		
R_r	20 mΩ	N	900		
L_r	150 mH	A	0.04		
p	3	i_0	0.88 A		
		Hydrogen Tank			
		M_0	5 kg		
		C_{tank}	10 kg		

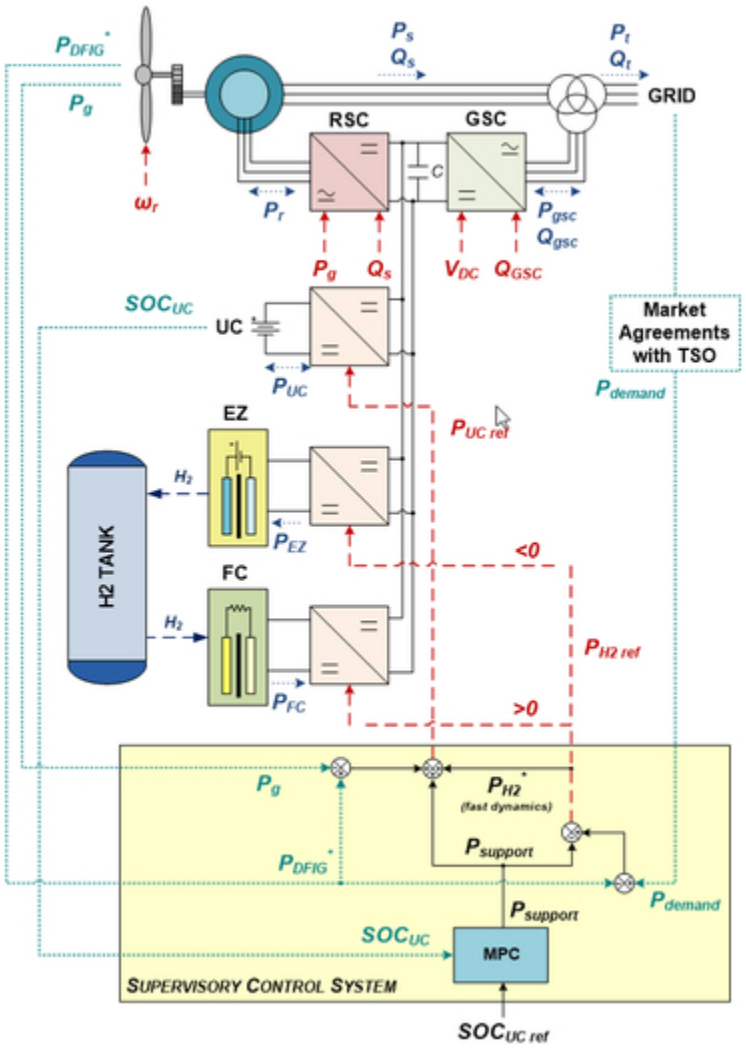

Figure 1: Scheme of the hybrid configuration proposed.

32x44mm (300 x 300 DPI)

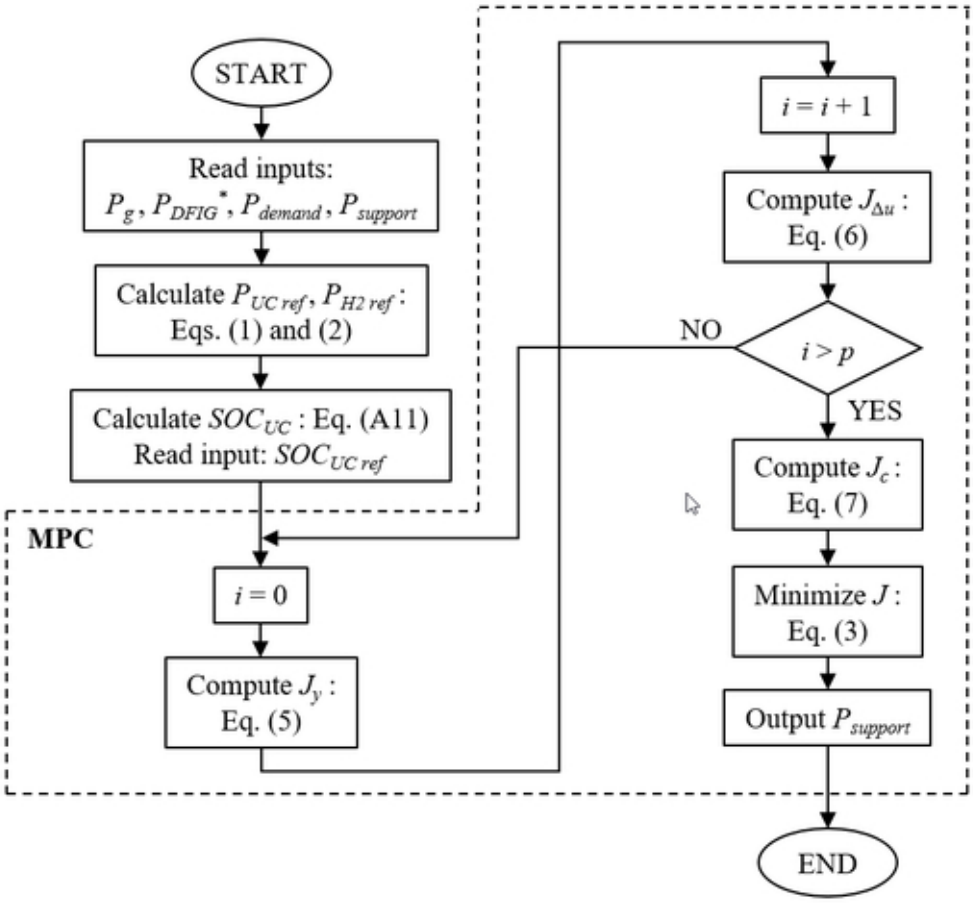

Figure 2: Flowchart of the SCS.

44x40mm (300 x 300 DPI)

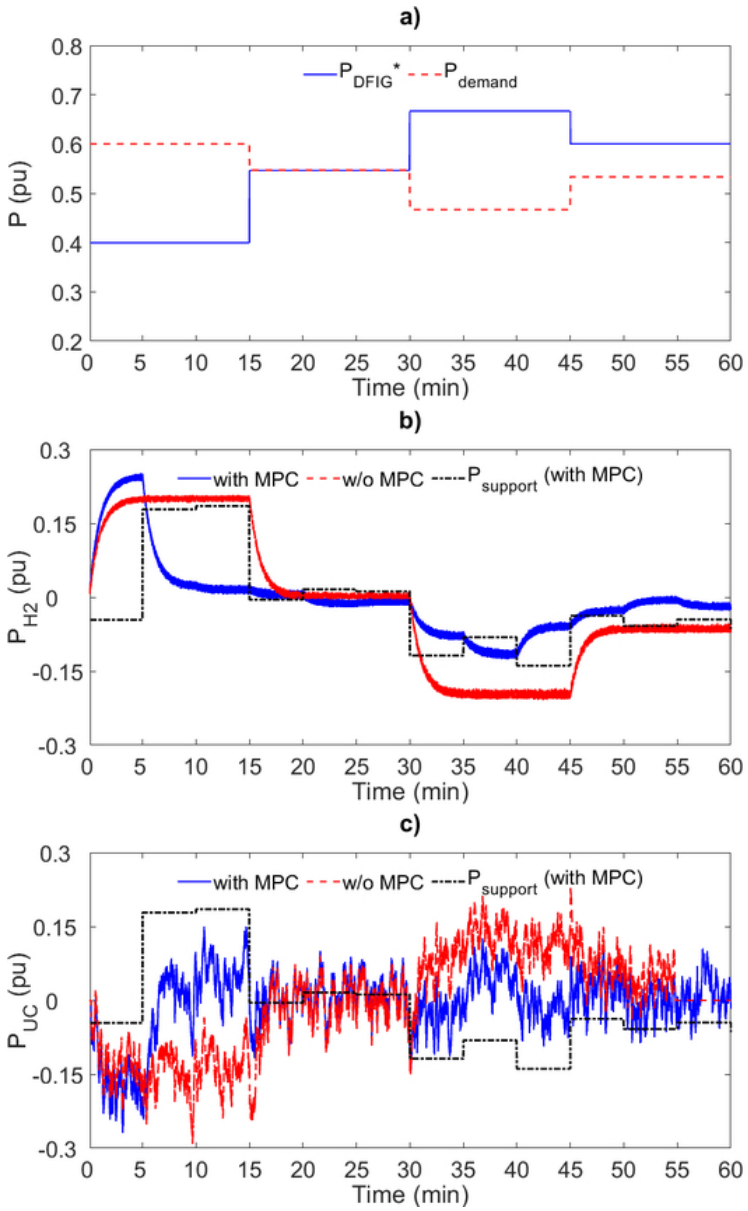

Figure 3: Results of case study 1: a) DFIG power generation forecast and Pdemand; b) Hydrogen system output power and Psupport; c) UC output power and Psupport.

45x72mm (300 x 300 DPI)

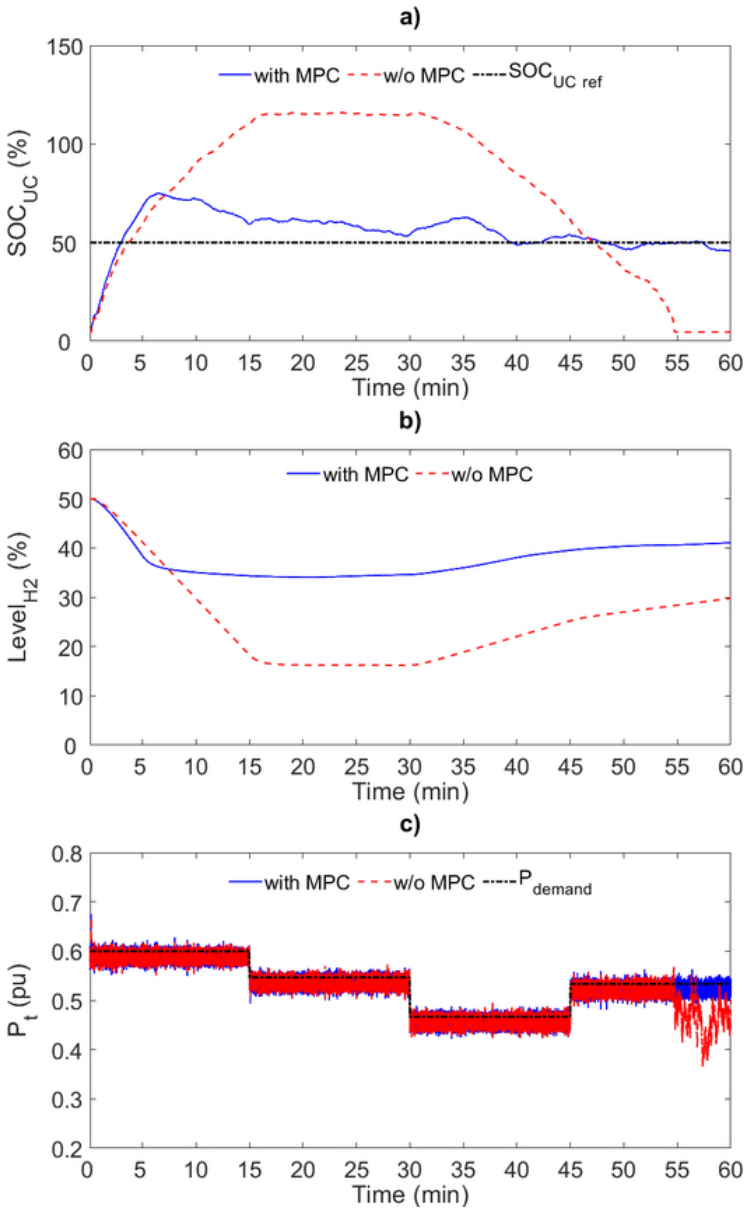

Figure 4: Results of case study 1 (cont.): a) SOC of the UC; b) Level of the hydrogen tank; c) Total output power of the hybrid system.

45x72mm (300 x 300 DPI)

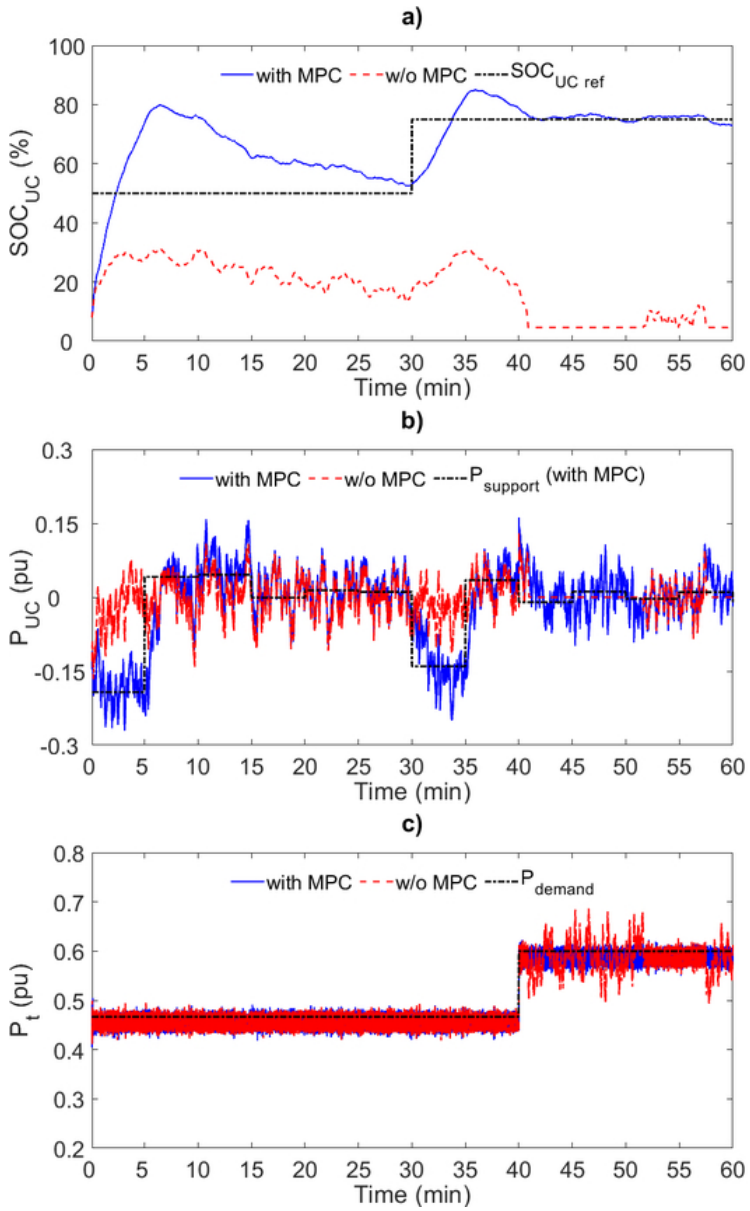

Figure 5: Results of case study 2: a) SOC of the UC; b) UC output power and Psupport; c) Total output power of the hybrid system and grid demand.

45x72mm (300 x 300 DPI)

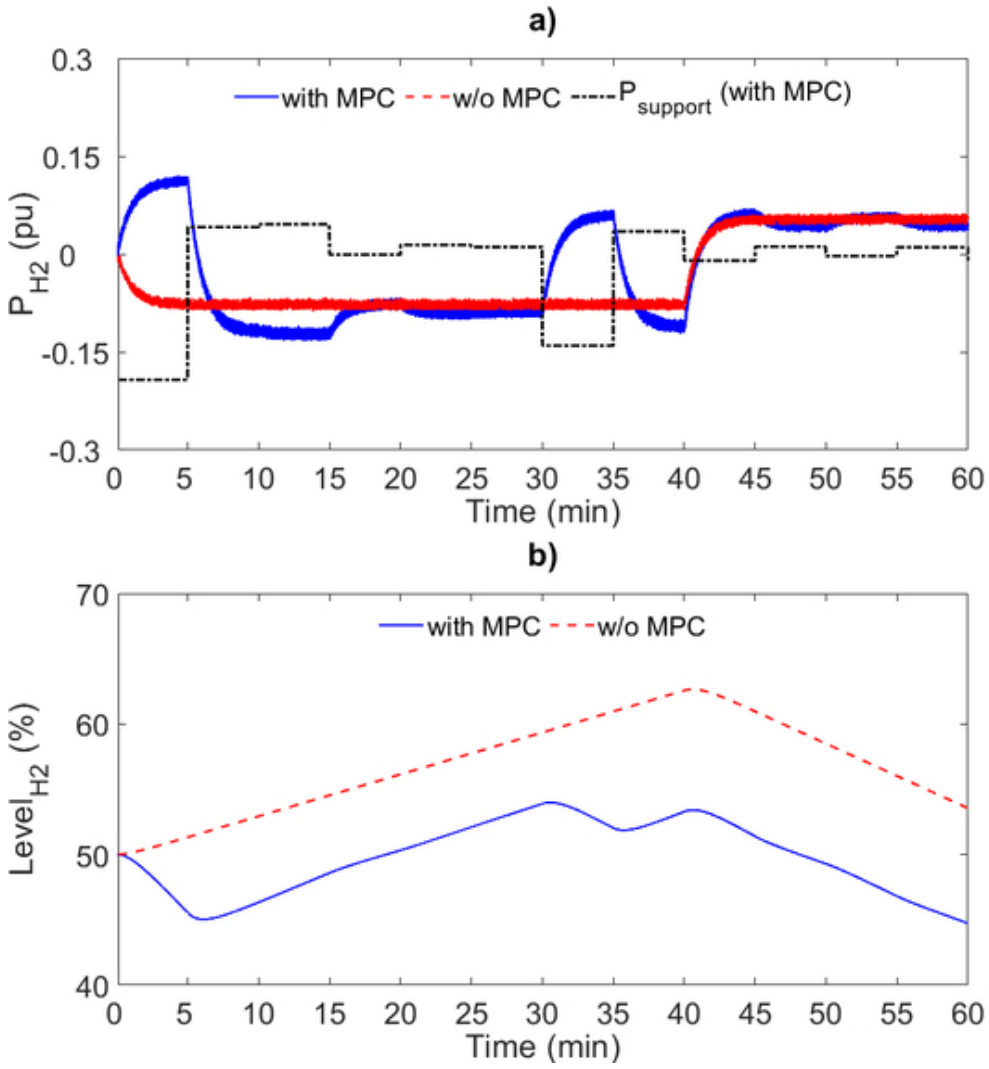

Figure 6: Results of case study 2 (cont.): a) Hydrogen system output power and Psupport; b) Level of the hydrogen tank.

45x48mm (300 x 300 DPI)